



Shear-SANS study of single-walled carbon nanotube suspensions

H. Wang^{a,*}, G.T. Christopherson^a, Z.Y. Xu^a, L. Porcar^b,
D.L. Ho^b, D. Fry^c, E.K. Hobbie^c

^a Department of Materials Science and Engineering, Michigan Technological University, 504 M&ME Bldg., 1400 Townsend Drive, Houghton, MI 49931, United States

^b NIST Center for Neutron Research, National Institute of Standards and Technology, Gaithersburg, MD 20899, United States

^c Polymers Division, National Institute of Standards and Technology, Gaithersburg, MD 20899, United States

Received 24 January 2005; in final form 31 August 2005

Abstract

We report a combined shear small-angle neutron scattering (shear-SANS) and rheo-optical study of dilute aqueous suspensions of SWNT bundles dispersed using ionic surfactants. Both shear-SANS and flow birefringence reveal weak shear-induced alignment of SWNT bundles along the direction of flow. In terms of a nematic order parameter, the degree of alignment is found to increase with the shear rate, reaching ca. 0.08 at 2000 s^{-1} . Addition of a soluble polymer to the SWNT suspensions diminishes shear-induced alignment. The factors limiting shear alignment in dilute SWNT suspensions are discussed.

© 2005 Elsevier B.V. All rights reserved.

Single-walled carbon nanotubes (SWNTs) are structurally unique materials that offer great promise for novel applications due to their excellent mechanical, electrical, thermal, and optical properties [1,2]. Much fundamental research aimed at achieving practical SWNT-based technologies has been explored [3], whereas studies directed at the flow processing of SWNTs in suspension are still rather limited [4,5]. A better understanding of the flow response of carbon-nanotube suspensions is important to establishing efficient processing schemes tailored to specific SWNT applications.

It is recognized that upon shearing, rod-like objects, such as multiwalled carbon nanotubes (MWNTs) [6–8] and tobacco mosaic virus (TMV) [9,10], can develop nematic order in suspensions. Much previous effort has focused on SWNT/polymer nanocomposites [11–14], and studies on concentrated aqueous suspensions of SWNT are possible due mostly to the recent discovery of an effective surfactant for SWNT dispersion [15]. Small-angle neutron scattering (SANS) is a suitable technique for characterizing SWNT aqueous suspensions. Previous SANS measure-

ments suggest both rigid-rod structures in dispersed SWNT suspensions [16,17], and an optimal surfactant concentration for dispersion [18]. This Letter reports details of the first neutron scattering experiment on the shear response of SWNTs dispersed in aqueous suspensions using ionic surfactants. Shear-induced alignment is quantified through an approximate nematic order parameter and compared with flow birefringence and rheological measurements.

Single-walled carbon nanotubes (SWNTs) synthesized through high pressure catalytic decomposition of carbon monoxide (HiPco) were obtained from Carbon Nanotechnology Inc.¹ As-received SWNTs were further purified through thermal oxidation at 260 °C and 1 M HCl solution reflux, and processed by ultrasonication in dilute nitric acid [19]. After repeatedly rinsing with deionized water, dried SWNTs appear as continuous fibers (Fig. 1g). The SWNT suspension consists of 0.08% SWNT and 0.6% sodium dodecylbenzenesulfonate (SDBS) [15] by mass in D₂O.

¹ Certain equipment, instruments or materials are identified in the Letter in order to adequately specify the experimental details. Such identification does not imply recommendation by the National Institute of Standards and Technology, nor does it imply the materials are necessarily the best available for the purpose.

* Corresponding author. Fax: +1 906 487 2934.
E-mail address: wangh@mtu.edu (H. Wang).

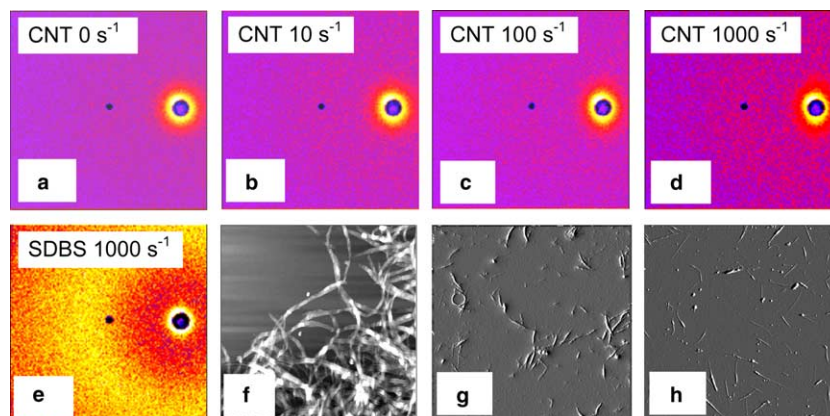


Fig. 1. 2D SANS intensity for the SWNT suspension at various shear rates (a)–(d) and for the 1% SDBS surfactant solution at the shear rate of 1000 s^{-1} (e). Anisotropic scattering in the CNT suspension is visible at high shear rates, whereas the surfactant solution remains isotropic at 1000 s^{-1} . (f)–(h) AFM scans of the SWNT bundles dried from solution on Si substrates (image size: $5 \times 5 \mu\text{m}$). (f) Continuous and entangled SWNT fibers after purification but before dispersion with surfactant. Height analysis indicates bundle diameters of 20–30 nm. (g) Isolated SWNT bundles after 10 h ultrasonic dispersion in SDBS solution, with diameters of 12–17 nm and lengths of ca. $0.8 \mu\text{m}$. (h) Fine SWNT bundles after 24 h ultrasonic dispersion, showing diameters of 4–8 nm and lengths of ca. $0.5 \mu\text{m}$. Only intermediate dispersion as in (g) results in detectable shear-induced alignment.

After ultrasonication in an ice bath for 10 h, the SWNTs exist in the suspension as bundles of diameter ranging from 12 to 17 nm, and lengths of about $0.5\text{--}1 \mu\text{m}$ (Fig. 1g). Better dispersion could be achieved by longer (48 h) ultrasonication, as shown in Fig. 1h. As a control, 1% SDBS surfactant solution in D_2O was also prepared. In another suspension, premixed SWNT/SDBS suspension and a 4% polyethylene oxide (PEO, $M_w = 10^6 \text{ g/mol}$) in D_2O solution were mixed to give 0.013% SWNT, 0.13% SDBS, and 2.67% PEO by mass.

Shear small-angle neutron scattering (shear-SANS) measurements were performed using the 8 m SANS instrument at the NIST Center for Neutron Research. Incident neutrons of wavelength $\lambda = 10 \text{ \AA}$ and a sample-to-detector distance of 3.84 m yielded a range of scattering wavevector, $0.006 \text{ \AA}^{-1} < Q < 0.1 \text{ \AA}^{-1}$. The neutron wavelength dispersion, $\Delta\lambda/\lambda = 0.15$, is mainly responsible for the resolution of the SANS measurement. For example, ΔQ_s are 0.0016 \AA^{-1} and 0.003 \AA^{-1} for Q_s of 0.007 and 0.05 \AA^{-1} , respectively. However, this finite Q -resolution has no effect on the data analysis because of the diffuse features of the SANS spectra in this study. A Couette-type shear instrument was used in this study. The outer diameter of the inner quartz stator and the inner diameter of the outer quartz rotor are 60 and 61 mm, respectively, giving a 0.5 mm gap between the two cylinders. This instrument covers a range of shear rates, $\dot{\gamma}$, from 0.05 to 2000 s^{-1} . The sample temperature was maintained at $25 \text{ }^\circ\text{C}$, which was controlled by a bath circulating through the stator. SANS measurements were made at various $\dot{\gamma}$, with the incident neutron beam in the gradient direction, perpendicular to the flow-vorticity plane. The scattered neutrons were counted with a 2D detector. The X and Y coordinates of 2D spectra represent the flow and vorticity directions, respectively. After correction for background and detector efficiency, and conversion to an absolute scale using the direct beam intensity, the 2D intensity was either circularly,

annularly, or rectangular-section averaged to yield the scattering cross section of the sample in the corresponding geometries.

Rheo-optical measurements were carried out using a Rheometrics rheometer¹ with plate-plate geometry and an optical attachment. The birefringence at $\lambda = 670 \text{ nm}$ and shear viscosity were recorded simultaneously as a function of $\dot{\gamma}$, from 2 to 8000 s^{-1} . At each $\dot{\gamma}$, data were acquired at a rate of 1 Hz and were averaged over 20 measurements.

Fig. 1 shows the 2D SANS intensity for the SWNT suspension at various $\dot{\gamma}$ s and for the SDBS surfactant solution at $\dot{\gamma} = 1000 \text{ s}^{-1}$. Anisotropic scattering in the SWNT suspension is visible at high rates of strain, whereas the surfactant solution remains isotropic at 1000 s^{-1} . As the SDBS forms micelles in solution, the intensity maxima at $Q = 0.052 \text{ \AA}^{-1}$ indicates the average spacing between micelles, about 120 \AA . However, this value is not sensitive to the surfactant concentration. For example, as the surfactant concentration increases by 10-fold, from 0.5% to 5%, the peak position slightly shifts to higher Q , with a change of ca. 15%. It is understood that in this ionic surfactant system, the dominant interactions between micelles are due to long range Coulombic forces rather than short range hard-wall interactions; as the force determines the average spacing, a change in overall concentration would reflect a change in the molecular packing density in individual micelles rather than the number density of micelles. This invariance is important in the analysis below for the SWNT suspension, in which the scattering contribution from surfactant molecules not adsorbed onto SWNT bundles is approximated as proportional to that from the pure SDBS solution.

Fig. 1 also shows AFM scans of the SWNT bundles dried from solution on Si substrates [(f)–(h), image size: $5 \times 5 \mu\text{m}$]. Fig. 1f shows continuous and entangled SWNT fibers after purification but before dispersion with surfactant. Height analysis indicates bundle diameters of 20–

30 nm. This is typical SWNT morphology before debundling. Fig. 1g shows isolated SWNT bundles after 10 h of ultrasonic dispersion in SDBS solution, with diameters of 12–17 nm and lengths of ca. 0.8 μm . Fig. 1h shows fine SWNT bundles after 48 h of ultrasonic dispersion, with diameters of 4–8 nm and lengths of ca. 0.5 μm . Only intermediate dispersion as in Fig. 1g results in a measurable degree of shear-induced alignment as shown in (a)–(d). Neither suspension with brief disruption of the bundle networks (in either room-temperature ionic liquids or surfactant solutions with brief ultrasonication) nor finely dispersed SWNT in solution [similar to (h) or better] results in detectable shear-induced anisotropy.

To analyze the effect of shear on the SWNT suspension, rectangular sections across the beam center in both the flow and vorticity directions were averaged to yield a 1D projection. Fig. 2 shows the SANS spectra obtained in this manner along the flow direction at 0 s^{-1} (filled circles) and 1000 s^{-1} (open squares). The intensity at low- Q is due to the surfactant-dispersed SWNTs and shows power-law dependence. The high- Q scattering comes from SDBS not adsorbed onto SWNT bundles and is invariant under shear, which is clearly revealed from radial averaging the entire 2D intensity. The reduced SDBS intensity compared to that of the neat surfactant solution is due both to the lower SDBS concentration after adsorption and poor statistics from rectangular sectioning. For comparison, the SANS spec-

trum of the 1% surfactant solution (open triangles) is also plotted in Fig. 2. In view of their distinct shear responses, neglecting the cross terms, the total scattering intensity is divided into three parts; power-law SWNT scattering, residual surfactant scattering scaled from its pure solution intensity, and an incoherent background,

$$\frac{d\Sigma}{d\Omega}(Q) = \left. \frac{d\Sigma}{d\Omega} \right|_{\text{SWNT}} + \left. \frac{d\Sigma}{d\Omega} \right|_{\text{SDBS}} + I_{\text{inc}} = \frac{I_0}{Q^\alpha} + pI_{\text{SDBS}}(Q) + I_{\text{inc}}, \quad (1)$$

where I_0 is the coefficient of the power law, α the power-law exponent, $I_{\text{SDBS}}(Q)$ the coherent scattering intensity of the pure SDBS solution, p a scaling prefactor, and I_{inc} the incoherent background. The solid lines are the best fits according to Eq. (1), with a power-law exponent of 2.85. This value falls into the range of 2–3 for a variety of SWNT suspensions and polymer composites, which is usually attributed to either network formation [4,16] or branching in SWNT bundles and a wide distribution of sizes and structures in the measurement window of 30–100 nm [20]. However, Q^{-1} power-law behavior from depolarized light scattering on the suspensions of interest here [inset (b)] implies that the SWNT bundles can indeed be approximated as rigid rods at large scales, while the magnitude of the SANS exponent more likely reflects the high Q -range of the measurement.

The inset (a) of Fig. 2 shows the coefficients, $I_{0,Y}$ and $I_{0,X}$, obtained from fitting for both the vorticity (filled triangles) and flow (open circles) directions, respectively. $I_{0,Y}$ remains relatively constant over a large range of the shear rates, and increases slightly at very high shear rates. On the other hand, $I_{0,X}$ decreases monotonically with shear rate. Under simple shear, SWNT bundles become aligned along the flow direction, giving rise to the higher scattering intensity in the transverse vorticity direction than in the flow direction. However, interestingly, the increase in $I_{0,Y}$ is rather modest; the increasing difference between $I_{0,X}$ and $I_{0,Y}$ is mainly due to the steady decrease in $I_{0,X}$. This could be qualitatively argued as follows. As tubes align along the flow direction X, the projection of length along X increases, resulting in a smaller intensity over the Q -range of the measurement, which is essentially for smaller length scales. On the other hand, the projected length along the Y direction does not fall in the Q -range of the detection window, from 0.006 to 0.02 \AA^{-1} .

The degree of SWNT alignment can be quantified with a nematic order parameter defined by Hermans's orientation function, $f = (3 \langle \cos^2 \phi \rangle - 1)/2$, where the angular average is approximately related to the anisotropic scattering intensity [21]. The angular scattering intensity $I(\phi)$ is obtained from the SANS spectra at $Q = 0.01 \text{\AA}^{-1}$ as a function of the azimuthal angle, ϕ . The nematic order parameters were calculated at $Q = 0.01 \text{\AA}^{-1}$ at various shear rates, as shown in Fig. 3. As the order parameter f ranges from 0 for random orientation to 1 for perfect alignment, even the best alignment for SWNT bundles in the suspension in this study ($f = 0.08$ at $\dot{\gamma} = 2000 \text{ s}^{-1}$) is rather modest.

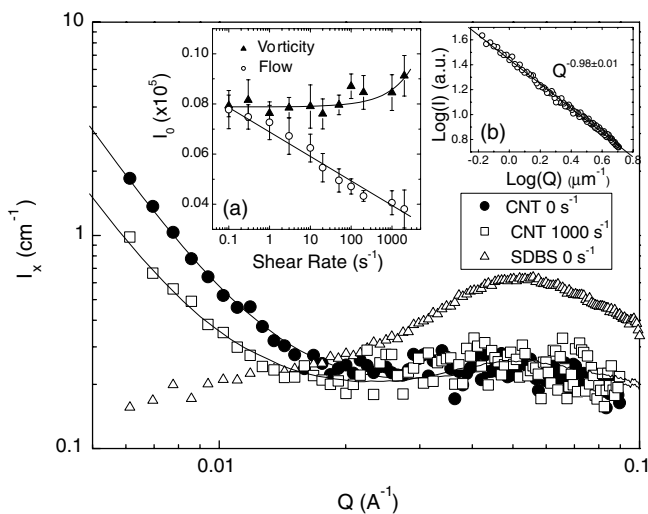


Fig. 2. Rectangular-section averaged SANS spectra in the flow direction for the CNT suspension at 0 (filled circles) and 1000 s^{-1} (open squares). The intensity decreases with shear rate at low- Q . The solid lines are the best fits according to Eq. (1). The SANS spectrum for 1% surfactant solution (open triangles) was used to account for high- Q scattering signals of the CNT suspension. The inset (a) shows the coefficients of the power law in both the vorticity (filled triangles) and flow (open circles) directions obtained from fitting. This coefficient remains relatively constant in the vorticity direction up to 100 s^{-1} , and increases slightly at higher shear rates. On the other hand, the coefficient in the flow direction decreases monotonically with shear rates. The inset (b) shows the light scattering intensity of the SWNT solution at quiescence in log-log scale. The Q^{-1} scattering law indicates rod-like behavior at large length scales.

The in situ shear-SANS studies were complemented with rheo-optical measurements. The inset (a) of Fig. 3 shows the flow birefringence, $\Delta n'$, for both the surfactant solution (triangles) and the SWNT suspension (circles). The surfactant solution shows negligible $\Delta n'$ over the entire range of the shear rates in this study, whereas $\Delta n'$ of the SWNT suspension increases with shear rate and reaches a maximum value of ca. 3.5×10^{-5} around 2000 s^{-1} . Since the SWNTs are anisotropic linear objects, the optical properties of their bundles, such as absorption, polarization, refraction and reflectance, strongly depend on the relative angle between the polarization direction and the nanotube symmetry axis [22]. A positive $\Delta n'$ indicates that SWNT bundles align along the flow direction, with the degree of alignment increasing with shear rate. This observation is consistent with shear-SANS results over the overlap range, $10 \text{ s}^{-1} < \dot{\gamma} < 2000 \text{ s}^{-1}$. The relationship $2\Delta n' \approx \delta' \phi f$, where δ' and ϕ are the dielectric anisotropy and volume fraction of SWNT bundles, respectively [23], gives δ' as approximately 1.5, which represents the difference in dielectric constant along and normal to the symmetry axis at $\lambda = 670 \text{ nm}$ for SWNT bundles in this study. We expect the measured dielectric anisotropy can be a function of the raw tube sample, the purification procedure, and the sample geometry.

The corresponding shear viscosity as a function of shear rate for both the pure surfactant solution (triangles) and the SWNT suspension (circles) is shown in inset (b). Below 1000 s^{-1} , a constant viscosity of 0.0009 Pa s was found for both the surfactant solution and the dilute SWNT suspen-

sion, which is comparable to the value of pure water. At higher shear rates, however, both the surfactant solution and the SWNT suspension show a slight increase in viscosity, suggestive of the onset of shear thickening, probably due to the initial stages of the formation of turbulent flow characteristics, such as eddies. This observation suggests that the addition of the SWNTs has little effect on the flow properties of the solution, as expected for dilute suspensions of this type.

Attractive interactions between nanotubes – coupled with the mechanical entanglement of high-aspect-ratio nanofibers – are responsible for the shear-induced flocculation previously reported in non-Brownian MWNT suspensions [8]. In the aqueous SWNT/SDBS suspensions of interest here, these effects are largely overcome by surfactant adsorption onto the SWNT surfaces; flocculation does not occur under shear. The weak SWNT alignment can be viewed as a direct consequence of three limiting factors. The physical geometry of the SWNT bundles (which are not strictly rod-like) may lower the effective aspect ratio and therefore inhibit strong flow alignment in simple shear. The low SWNT concentration also limits flow-induced tube-tube interactions. Furthermore, the low viscosity of the solvent limits the measurement to a range of Peclet numbers where disordering thermal effects are still relevant. A further test of the importance of these three effects on flow-induced SWNT alignment, as well as their potentially complicated interplay, is demonstrated by shear-SANS measurements on the SWNT-PEO suspensions. The 2D SANS scattering patterns at quiescence and at $0.1 < \dot{\gamma} < 1000 \text{ s}^{-1}$ are shown in Fig. 4. The scattering patterns all look similar and isotropic and the corresponding radially averaged scattering intensities are identical within experimental errors, which are of the symbol size. Anisotropic scattering is not observed, implying a complete lack of shear-induced SWNT orientation. Although the addition of soluble polymer increases the solvent viscosity, it also introduces a strong tube-tube attraction which leads to flocculation in quiescence, which limits the ability of the shearing forces to align the nanotubes.

In summary, we report a combined shear-SANS and rheo-optical study of a suspension of SWNT bundles in heavy water. Both the 2D shear-SANS pattern and the flow birefringence indicate shear-induced alignment of SWNT bundles in the flow direction. This, however, occurs only in an intermediate range of dispersing and debundling of SWNTs. Neither brief nor deep dispersion led to observable shear-alignment of SWNTs in suspension. For brief dispersion, much of the morphology as shown in Fig. 1f is retained, and a shear effect is simply not expected. On the other hand, better dispersion could result in rod-like tubes or thin bundles at the cost of short tube lengths and severe tube damages, causing lower Peclet numbers and hence limited shear-induced effects. Competition between these factors results in a narrow processing window for any shear-alignment, the degree of which is rather modest. A high degree of shear-induced SWNT alignment will require

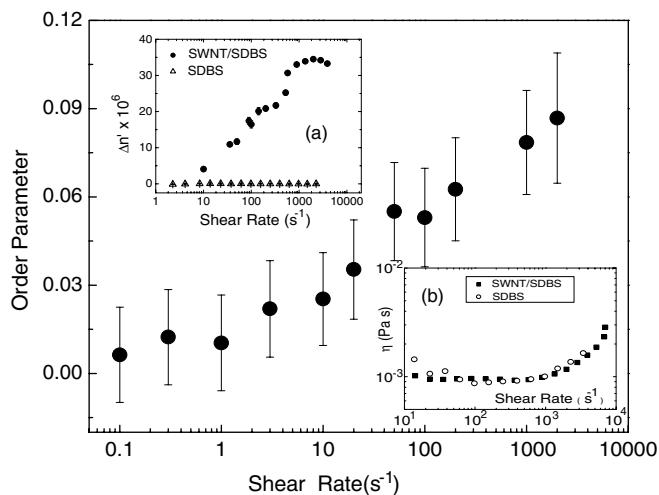


Fig. 3. The approximate nematic order parameter calculated from the annularly averaged SANS data at $Q = 0.01 \text{ \AA}^{-1}$. The inset (a) shows the flow birefringence for both the surfactant solution (triangles) and the SWNT suspension (circles). The surfactant solution shows zero flow birefringence, whereas that of the SWNT suspension increases with shear rate up to around 2000 s^{-1} . The flow birefringence closely traces the order parameter in the overlap range of shear rates. The inset (b) shows the viscosity as a function of the shear rate for both the SWNT suspension (filled squares) and the neat surfactant solution (open circles). A constant viscosity of ca. 0.0009 Pa s was observed below 1000 s^{-1} . The increase at higher shear rate may indicate the onset of shear thickening due to the turbulent flow.

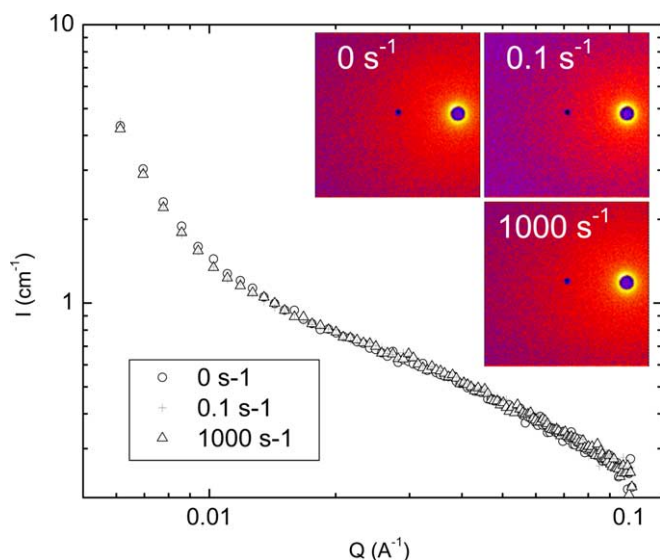


Fig. 4. 2D SANS patterns for the SWNT-PEO suspension at various shear rates, and the corresponding radially averaged scattering intensities. The scattering profiles are identical within experimental errors, which are of the symbol size. Anisotropic scattering is not observed up to a high shear rate of 1000 s^{-1} .

dispersing straight tubes with large aspect ratios at high concentrations in very viscous solvents at high rates of strain.

Acknowledgments

H.W. acknowledges the NSF Career Award DMR-0348895, NIST award 70NANB3H1130, the faculty start-up fund from Michigan Technological University, and the support of the National Institute of Standards and Technology in providing the neutron research facilities used in this work.

References

- [1] R. Saito, G. Dresselhaus, M.S. Dresselhaus, *Physical Properties of Carbon Nanotubes*, Imperial College Press, London, 1998.
- [2] R.H. Baughman, A.A. Zakhidov, W.A. de Heer, *Science* 297 (2002) 787.
- [3] S.B. Sinnott, R. Andrews, *Crit. Rev. Solid State Mater. Sci.* 26 (2001) 14.
- [4] L.A. Hough, M.F. Islam, P.A. Janmey, A.G. Yodh, *Phys. Rev. Lett.* 93 (2004) 168102.
- [5] V.A. Davis, L.M. Ericson, A.N.G. Parra-Vasquez, H. Fan, Y. Wang, V. Prieto, J.A. Longoria, S. Ramesh, R.K. Saini, C. Kittrell, W.E. Billups, W.W. Adams, R.H. Hauge, R.E. Smalley, M. Pasquali, *Macromolecules* 37 (2004) 154.
- [6] E.K. Hobbie, H. Wang, S.D. Hudson, C.C. Han, J. Obrzut, *Rev. Sci. Instr.* 74 (2003) 1244.
- [7] E.K. Hobbie, H. Wang, H. Kim, S. Lin-Gibson, S.D. Hudson, C.C. Han, E.A. Grulke, *Phys. Fluids* 15 (2003) 1196.
- [8] S. Lin-Gibson, J.A. Pathak, E.A. Grulke, H. Wang, E.K. Hobbie, *Phys. Rev. Lett.* 92 (2004) 048302.
- [9] U.T. Reinhardt, E.L.M. de Groot, G.G. Fuller, W.M. Kulicke, *Macromol. Chem. Phys.* 196 (1994) 63.
- [10] J. Penfold, *J. Appl. Cryst.* 21 (1988) 770.
- [11] F.M. Du, J.E. Fischer, K.I. Winey, *J. Polym. Sci. B Polym. Phys.* 41 (2003) 3333.
- [12] C. Park, Z. Ounaies, K.A. Watson, R.E. Crooks, J. Smith Jr., S.E. Lowther, J.W. Connell, E.J. Siochi, J.S. Harrison, T.L. St. Clair, *Chem. Phys. Lett.* 364 (2002) 303.
- [13] S. Kumar, T.D. Dang, F.E. Arnold, A.R. Bhattacharyya, B.G. Min, X.F. Zhang, R.A. Vaia, C. Park, W.W. Adams, R.H. Hauge, R.E. Smalley, S. Ramesh, P.A. Willis, *Macromolecules* 35 (2002) 9039.
- [14] C.A. Mitchell, J.L. Bahr, S. Arepalli, J.M. Tour, R. Krishnamoorti, *Macromolecules* 35 (2002) 8825.
- [15] M.F. Islam, E. Rojas, D.M. Bergey, A.T. Johnson, A.G. Yodh, *Nano Lett.* 3 (2) (2003) 269.
- [16] W. Zhou, M.F. Islam, H. Wang, D. Ho, A.G. Yodh, K.I. Winey, J.E. Fischer, *Chem. Phys. Lett.* 384 (2004) 185.
- [17] K. Yurekli, C.A. Mitchell, R. Krishnamoorti, *J. Am. Chem. Soc.* 126 (2004) 9902.
- [18] H. Wang, W. Zhou, D.L. Ho, K.I. Winey, J.E. Fischer, C.J. Glinka, E.K. Hobbie, *Nano Lett.* 4 (2004) 1789.
- [19] W. Zhou, Y.H. Ooi, R. Russo, P. Papanek, D.E. Luzzi, J.E. Fischer, M.J. Bronikowski, P.A. Willis, R.E. Smalley, *Chem. Phys. Lett.* 350 (2001) 6.
- [20] D.W. Schaefer, J.M. Brown, D.P. Anderson, J. Zhao, K. Chokalingam, D. Tomlin, J. Ilacsy, *J. Appl. Cryst.* 36 (2003) 553.
- [21] P.H. Hermans, J.J. Hermans, D. Vermaas, A.J. Weidinger, *J. Polym. Sci.* 3 (1947) 393.
- [22] M.F. Lin, *Phys. Rev. B* 62 (2000) 13153.
- [23] E.K. Hobbie, *J. Chem. Phys.* 121 (2004) 1029.